DOI: 10.1002/chem.200902517

Platinum Nanoparticles: The Crucial Role of Crystal Face and Colloid Stabilizer in the Diastereoselective Hydrogenation of Cinchonidine

Erik Schmidt, Wolfgang Kleist, Frank Krumeich, Tamas Mallat, and Alfons Baiker*[a]

Abstract: The preparation of stable metal nanoparticles requires a strong interaction between the (organic) stabilizer and the metal surface that might alter the catalytic properties. This behavior has been described as "poisoning" since the stabilizer normally decreases the catalytic activity due to site blocking. Here we show a striking influence of the stabilizer on the selectivity in the hydrogenation of cinchonidine (CD) over poly(acrylic acid) (PAA)-stabilized Pt nanoparticles with well-defined shape distributions. In the hydrogenation of the heteroaromatic ring of cinchonidine in toluene, the diastereomeric excess of the (*S*)-hexahydrocinchonidine increased upon increasing Pt{111}/Pt{100} ratio, but this distinct shape selectivity was observed only after the oxidative removal of PAA at 473 K. The use of the as-prepared nanoparticles inverted the major diastereomer to *R*, and this isomer was formed also in acetic acid. This striking change in the diastereoselectivity indicates that poly(acrylic acid), which remains on the Pt surface after preparation, interacts with CD during hydrogenation almost as strongly as the solvent acetic acid. The PAA stabilizer plays a dual role: it allows one to control the size and shape of the nanoparticles during their synthesis, and it affects the rate and diastereoselectivity of the hydrogenation of CD probably through a "surface-localized acidification".

Keywords: colloids · heterogeneous catalysis · hydrogenation · nanoparticles · selectivity

Introduction

Metal nanoparticles have been the target of intensive research in the past decades due to their intriguing chemical[1] and physical[2,3] properties. The unique features of these "metals in the embryonic state"[4] are reflected also in catalysis.[5–8] Nanoparticles of narrow size distribution[9–13] and those exhibiting preferentially exposed crystal facets[14–22] are attractive models for the investigation of the fundamental nature of active sites.

A key point in any application is the stability of the nanoparticles. In classical heterogeneous catalysis, the nanosized metal particles are stabilized by a high surface area support, and a similar role is played by the organic stabilizers (or capping agents) used for nanoparticles. When considering a conventional supported metal catalyst, the support may have a remarkable influence on the catalytic properties of the metal.[23–28] An analogous or even stronger effect is expected for the stabilizer that is present in considerable amounts on the surface of the nanoparticles but its interaction with the metal surface and the reactant is still poorly understood. It has been shown by comparing various stabilizers that there is an inverse correlation between the stability and the catalytic activity of nanoparticles.[9] In general, the strongly adsorbing stabilizer may have a negative effect on the catalytic activity due to site blocking. In addition, the selectivity of the catalytic reaction may be affected in different ways by the capping agent: 1) it may have a steric effect due to preferential adsorption on certain surface sites (analogous to selective poisoning[29]); 2) it may influence the electronic properties of the metal; and 3) interaction of the capping agent with the reactant can change the adsorption mode of the latter and its reactivity toward one of the products.

Here we report a striking effect of poly(acrylic acid) (PAA) stabilizer on the catalytic performance of Pt nanoparticles. We chose the practically relevant hydrogenation of the natural alkaloid cinchonidine (CD; see Scheme 1). This alkaloid is the most commonly used chiral modifier of Pt-group metals in heterogeneous asymmetric hydrogenation reactions.[30–33] CD adsorbs strongly on the Pt surface

[a] E. Schmidt, Dr. W. Kleist, Dr. F. Krumeich, Dr. T. Mallat, Prof. Dr. A. Baiker
Department of Chemistry and Applied Biosciences
ETH Zurich, Institute for Chemical and Bioengineering
Honggerberg, HCI, C8093 Zurich (Switzerland)
Fax: (+41) 44-632-1163
E-mail: baiker@chem.ethz.ch

Supporting information for this article is available on the WWW under http://dx.doi.org/10.1002/chem.200902517.

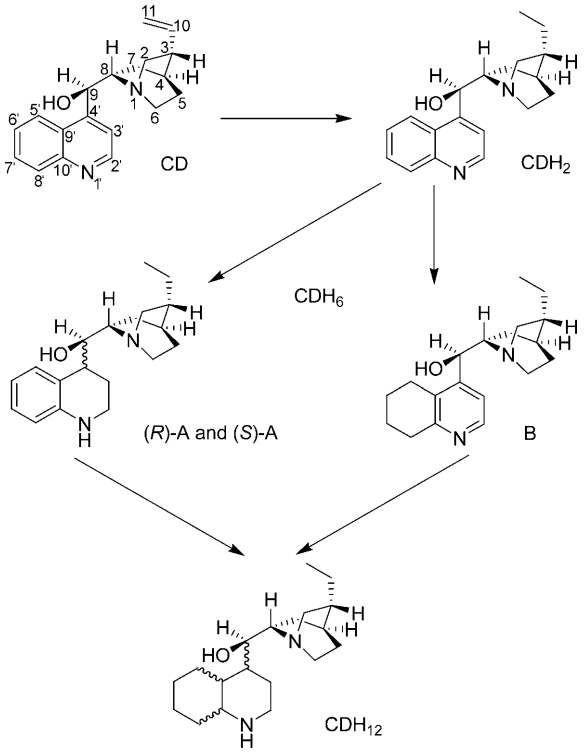

Scheme 1. Hydrogenation of cinchonidine (CD).

through the quinoline ring, a key requirement for inducing enantioselection at the metal surface.[34–37] An important side reaction that limits the application of cinchona alkaloids is the saturation of the quinoline ring, which leads to weaker adsorption on the metal surface and a considerable loss of enantiomeric excess.[38–40]

Results and Discussion

Structural and chemical properties of Pt nanoparticles

Characterization by electron microscopy: Representative electron micrographs of the nanoparticles are shown in Figure 1. The metal particles of all samples exhibit a narrow size distribution and a similar average diameter (d_{av}) of approximately 10 nm. The majority of the Pt particles in Pt-1 have a cube-like shape with preferentially exposed {100} faces, whereas Pt-3 consists of octahedral and truncated octahedral particles that expose especially {111} faces. Pt-2 exhibits a high amount of cubooctahedral particles with extended {100} and {111} faces.

A metal dispersion of 0.14 (Table 1) was calculated for all three samples (after supporting them onto silica) based on the particle size and shape distributions determined by counting 800–1000 particles for each sample.[41–43] The data agree well with those available in the literature.[10,14,17,21,43,44] Importantly, no change in the average particle size and in the shape distribution was observed after supporting the Pt colloids (TEM pictures in Figure 1, inset) onto silica (scanning transmission electron microscopy (STEM) pictures in Figure 1). Clearly, the method allows variation of the dominant crystallographic face of Pt while keeping the particle size virtually constant. This is an important condition for the unambiguous interpretation of the catalytic results.

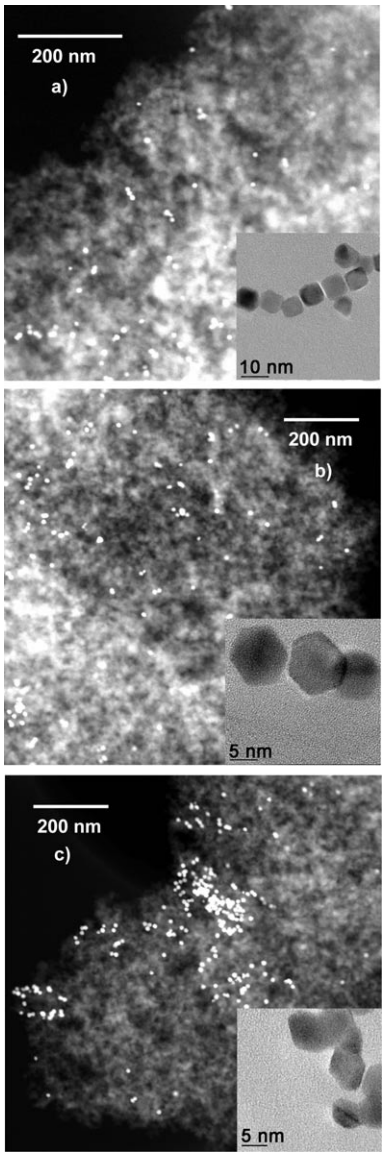

Figure 1. Representative STEM images of the silica-supported nanoparticles a) Pt-1, b) Pt-2, and c) Pt-3. The insets show TEM pictures of the parent colloids in aqueous solution.

Table 1. Characteristics of Pt nanoparticles supported on silica and those of the reference catalyst; "as-prepared" samples.

Sample	Pt [wt %]	d_{av} [nm]	Shape	Dispersion
Pt-1	0.78±0.10	9.8±1.1	cubic	0.14
Pt-2	0.70±0.08	9.8±0.8	cubooctahedral	0.14
Pt-3	0.68±0.08	10.2±1.2	hexagonal	0.14
Pt/Al_2O_3	5.8±0.3	3.2±1.2	spherical	0.32

Compared to the Pt nanoparticles, the particle-size distribution of the reference catalyst Pt/Al_2O_3 is broader but the

particles are smaller, thereby resulting in a higher dispersion of 0.32 (Table 1).

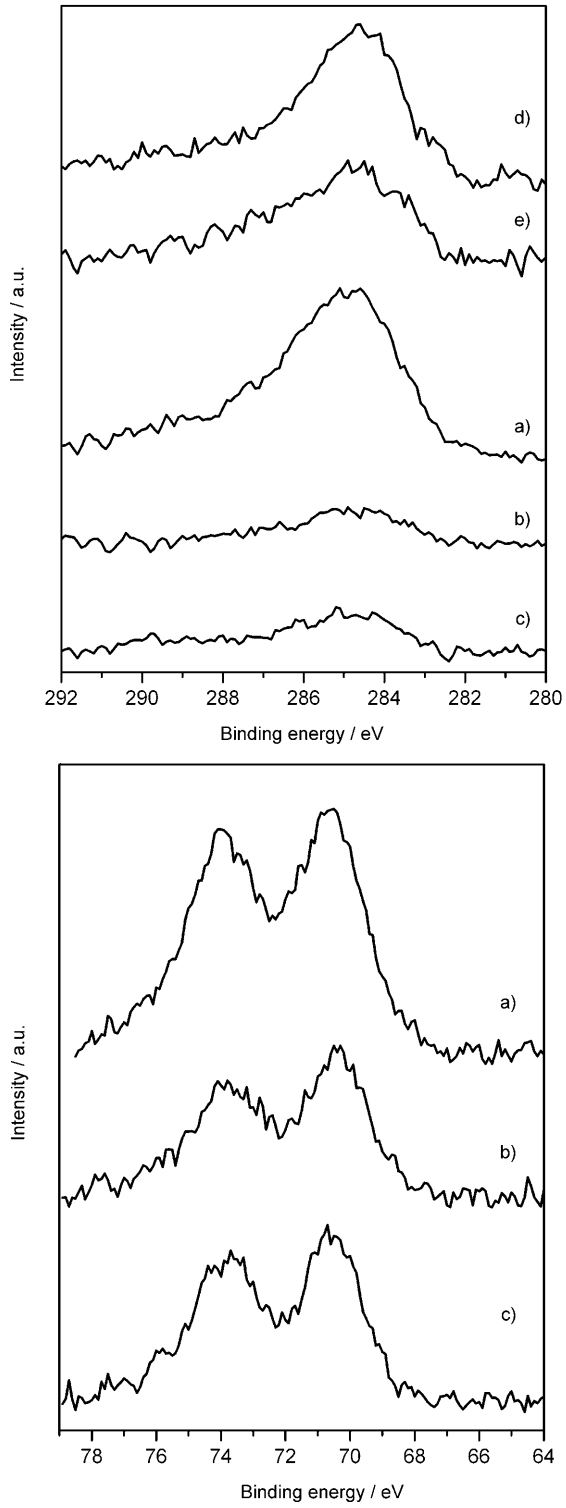

Figure 2. X-ray photoelectron spectra in the C 1s (top) and Pt 4f (bottom) regions. Spectra a, b, and c are related to Pt-1, Pt-2, and Pt-3, respectively. The PAA-treated neat silica belongs to spectra d and e (washed).

X-ray photoelectron spectroscopy (XPS): XPS measurements were performed to evaluate the presence of the organic stabilizer PAA on the Pt surface after deposition of the colloids onto the support. For comparison, a blank experiment was also made with pure silica without addition of Pt (Figure 2). The peak positions (Table 2) for Si 2p, O 1s, Pt $4f_{7/2}$, and C 1s in all samples are in agreement with literature data for silica, Pt^0, and poly(acrylic acid), respectively.[45] The unwashed silica reference material and Pt-1 showed an additional weak Cl signal (2s) at 265.2 and 265.5 eV, respectively. This chlorine impurity was probably introduced by setting the pH with aqueous HCl during deposition of the nanoparticles onto silica. The catalytic results indicate, however, that the presence of chlorine did not have a significant effect (see the section on catalytic behavior below).

The surface compositions (Table 2) were determined using the integral intensities of the characteristic peaks and the empirical cross-section factors for each element. All samples contained significant amounts of carbon, the main source of which is probably some residual colloid stabilizer PAA. For the three nanoparticles, the C/Pt atomic ratio varies in the range of 6–15. The large amounts of the same carbon species on the surface of the silica support even after washing with water suggests that the polymer residue in the supported nanoparticles is partially located on the silica support and the coverage of Pt by the stabilizer cannot be estimated from these data.

In summary, the XPS analysis proved that a considerable amount of the colloid stabilizer PAA was present on the surface of supported Pt nanoparticles despite the extensive washing with water, the reaction medium during catalyst synthesis.

Diffuse reflectance infrared spectroscopy (DRIFTS) study of CO adsorption: Adsorption of CO followed by DRIFTS was used to investigate the accessibility and morphology of the Pt surface. The spectra obtained on all samples, before and after pretreatment, are presented in Figure 3. The reference Pt/Al_2O_3 was diluted tenfold with KBr to account for the higher Pt content and dispersion. Still, the stretching vibration signals of adsorbed CO (spectra (a) in Figure 3A–D) are remarkably more intensive on the diluted Pt/Al_2O_3 compared to the nanoparticles (all deposited onto silica).

CO adsorption on Pt/Al_2O_3 (Figure 3A) is characterized by two main IR signals: one at around 2070 cm^{-1}, commonly attributed to a linear, single-bonded (on-top) species, and a second broader and less intensive signal at 1850 cm^{-1} that corresponds to bridge-bound CO.[46,47] The high-energy signal is split into a narrow, intensive signal at around 2085 cm^{-1} and a broad band at around 2050 cm^{-1}. The first signal is assigned to CO bound to highly coordinated Pt atoms such as {111} and {100} terraces, whereas the latter signal is attributed to CO adsorbed on low-coordinated Pt sites at step edges, corners, and defects.[48–51]

CO adsorption on Pt-1, Pt-2, and Pt-3 gave rise to very different IR signals. As seen from the spectra in Figure 3B–

Table 2. XPS analysis of the silica-supported Pt nanoparticles ("as-prepared") and the silica support treated with poly(acrylic acid) (PAA).

Sample	Peak positions [eV] (Composition [%])						
	Si		O	Pt		C	Cl
	2s	2p	1s	$4f_{7/2}$	$4f_{5/2}$	1s	2s
silica + PAA	154.4	103.4 (20.1)	532.8 (78.9)	–	–	284.7 (0.60)	265.2 (0.40)
silica + PAA, washed	154.4	103.4 (20.2)	532.7 (79.4)	–	–	285.0 (0.30)	– (0.13)
Pt-1	154.4	103.4 (20.2)	532.6 (79.1)	70.7 (0.02)	73.9	284.9 (0.30)	265.5 (0.38)
Pt-2	154.4	103.4 (20.2)	532.7 (79.7)	70.5 (0.02)	73.8	284.9 (0.11)	(trace)
Pt-3	154.4	103.4 (20.5)	532.8 (79.4)	70.6 (0.02)	73.9	284.8 (0.13)	(trace)

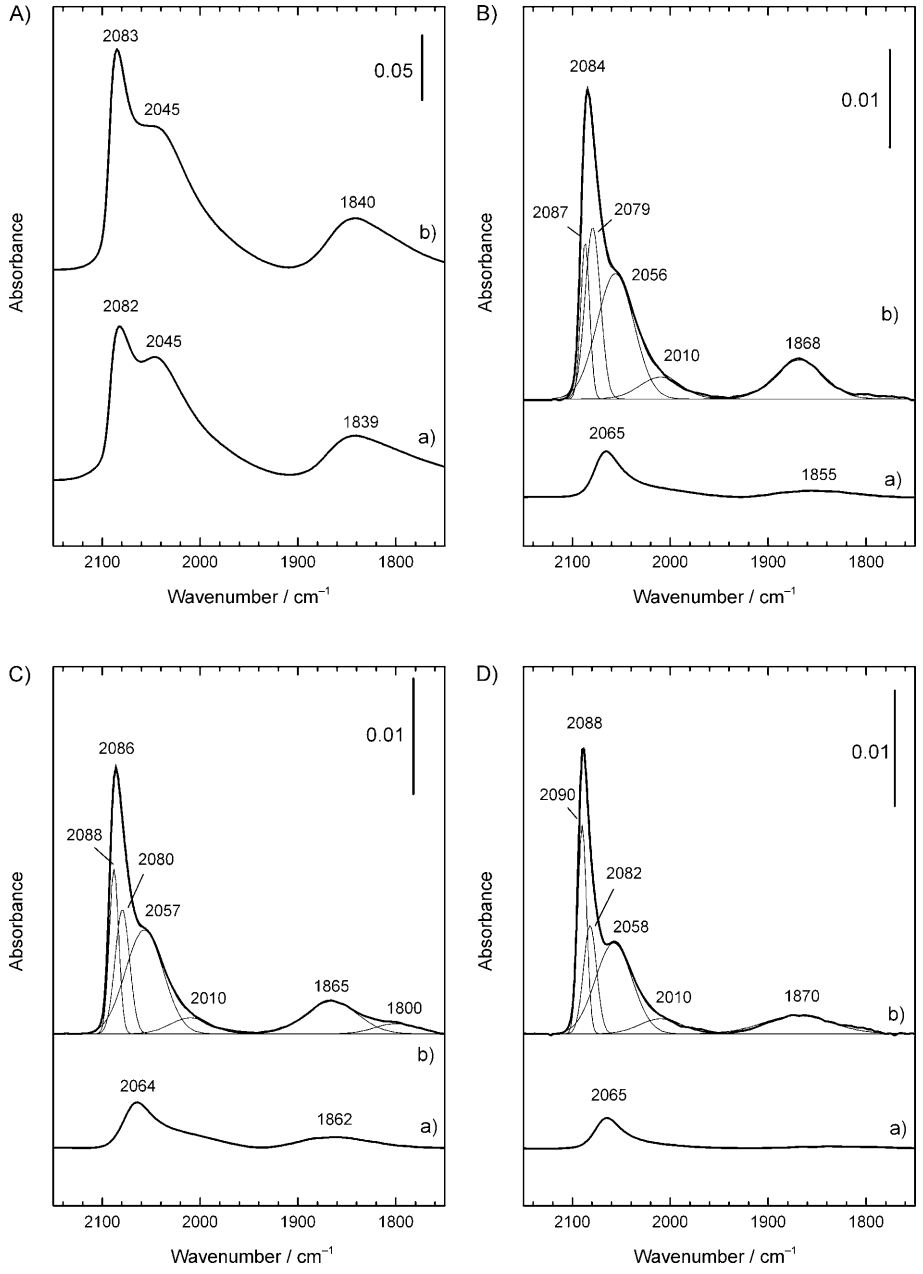

Figure 3. DRIFT spectra measured after CO adsorption on A) the reference catalyst Pt/Al_2O_3 and on supported nanoparticle samples B) Pt-1, C) Pt-2, and D) Pt-3. Spectra were collected after CO adsorption without any catalyst pretreatment (spectra a), and after treatment in O_2 and subsequently in H_2 at 473 K (spectra b).

D, lines (a) exhibit a weak signal at 2064–2065 cm^{-1} (at saturation coverage) independent of the particle shape. The signal is assigned to on-top CO on Pt terraces but is redshifted by 20–30 cm^{-1} relative to those on single crystals[52–55] and on Pt/Al_2O_3. Since all three samples exhibit a narrow size distribution with an average of 9–10 nm, the variation in the frequency of the on-top CO species due to different particle sizes[49] can be ruled out. The higher mean particle size of the nanoparticles compared to that of Pt/Al_2O_3 is expected to result in a smaller contribution of CO adsorbed on Pt defect sites and more pronounced, slightly blue-shifted on-top CO signals on terrace sites.[49] Taking into account the low intensity of the CO signals, the observed redshift can be explained by the very low CO coverage. The occupation of far-separated sites hinders dipole–dipole coupling and results in a lower C–O stretching frequency. Krebs and Lüth[55] observed a frequency of 2068 cm^{-1} for CO adsorption on Pt{111} at very low coverage. The signal was attributed to isolated CO species separated from each other by about 10 lattice constants. Also, Borchert et al. observed a redshift of 20–25 cm^{-1} on oxide-supported Pt nanoparticles capped with dodecylamine or hexanethiol.[56]

Only very small amounts of bridge-bound CO are seen also on Pt-1 and Pt-2 at 1855 and 1862 cm^{-1}, respectively. Clearly, the Pt surface is partly covered by contaminants on all three as-prepared nanoparticle samples and CO cannot efficiently compete for the surface Pt sites at the solid/gas interface.

A combined oxidative–reductive pretreatment at 473 K was effective in removing the surface residue of the stabilizer (Figure 3B–D). It increased the intensity of the signals of on-top CO by a factor of ten but also enhanced the signal of bridge-bound CO. The control experiment with Pt/Al_2O_3 revealed no significant difference

compared with the spectrum taken on the as-received sample (Figure 3A). After the combined pretreatment, the shape and intensity of the CO adsorption bands on the nanoparticles and on Pt/Al_2O_3 are similar and correspond well to literature data.[50] The frequency of the signal of CO linearly adsorbed on terrace sites is blueshifted by 20–25 cm^{-1} compared to the as-prepared samples. This shift is seen with all three nanoparticles and is due to higher CO coverage. A comparison of the three nanoparticles after the combined pretreatment reveals a slight blueshift from 2084 cm^{-1} (Pt-1) to 2086 cm^{-1} (Pt-2) to 2088 cm^{-1} (Pt-3). The shift is a consequence of the increasing {111}/{100} ratio and it is in excellent agreement with former studies.[57]

Deconvolution of the bands corroborates that variation of the particle shape was preserved after the oxidative–reductive pretreatment procedure (Figure 3B–D, Table 3). The ratio of {111}/{100} faces, as estimated from the signal intensities obtained by band deconvolution, increases from 0.9 for Pt-1 to 1.3 for Pt-2 and to 2.0 for Pt-3. This trend agrees well with the results of electron microscopy on the as-prepared samples,[43] thus indicating that changes in surface morphology of the Pt nanoparticles by the pretreatment in O_2 and H_2 are negligible (see Figure 4b). Literature reports on pretreatments in H_2 or O_2 affecting the shape of Pt nanoparticles are based on experiments at higher temperatures, typically at or above 923 K.[58–60]

The amount of defect and low-coordinated Pt sites relative to that of terraces cannot be quantified from the CO adsorption due to differences in the molecular IR absorption coefficients.[61,62] Nonetheless, the amount of defect sites relative to terraces is very similar for all nanoparticle samples (Table 3).

The IR spectra contain some further important information on the chemical nature of the surface species that acts as a poison to CO adsorption. The effect of the combined oxidative–reductive pretreatment is highlighted by the difference spectra obtained before and after pretreatment (Figure 5). Negative signals in these difference spectra indicate the removal of surface species during the treatment, and positive signals point to the formation of new species. The spectra in the fingerprint region show the removal of water as a broad negative signal at around 1630 cm^{-1}. Further negative signals at 1552 cm^{-1}, and less clearly pronounced at 1452 and 1401 cm^{-1}, correspond to strong positive signals in the spectrum of the neat PAA stabilizer (Figure 5, spectrum d) and can be assigned to the characteristic vibration of carboxylic groups and C–H deformational vibrations. This is a confirmation that the Pt surface was covered by the poly(carboxylic acid)-type stabilizer PAA that was removed by decarboxylation during the oxidative pretreatment. Note that Gomes et al. used 1% Pt/C as an effective decarboxylation catalyst with oxygen at 473 K.[63]

The difference spectra in the C–H stretching region (2700–3050 cm^{-1}; see Figure S1 in the Supporting Information) underline our interpretation. Therein the removal of hydrocarbon species is indicated by the strong negative signals at 2958, 2925, and 2854 cm^{-1}, respectively. The corresponding signals in the spectrum of the neat stabilizer are attributed to the symmetric and asymmetric stretching vibrations of the methylene groups of PAA. This is an indication that the intact stabilizer molecules rather than degradation species covered the Pt surface prior to the oxidative treatment.

A very weak positive signal at 2760 cm^{-1} in the difference spectra (Figure S1), not seen in the PAA spectrum, points to the formation of a new surface species during the oxidative–reductive treatment. The signal arises from C–H stretching vibrations of hydrocarbon methylene groups on the Pt surface.[66] It therefore indicates that even after the combined oxidative and reductive pretreatment procedure minor amounts of hydrocarbon fragments still remain on the Pt surface. Nevertheless, their impact on CO adsorption from the gas phase is negligible, as shown by the comparison with the reference Pt/Al_2O_3 catalyst.

Table 3. Characteristic data of CO adsorption after a combined oxidative–reductive pretreatment at 473 K (based on the band deconvolution of DRIFT spectra), and some selected literature values.

Species	Sample	Signal position [cm^{-1}]	fwhm[a] [cm^{-1}]	Intensity
CO linearly adsorbed on Pt{111} terraces	Pt-1	2087	10.5	0.016
	Pt-2	2088	11.2	0.014
	Pt-3	2090	10.5	0.018
	Pt/Al_2O_3	2085[b]	n.d.[c]	n.d.[c]
	lit. values	2087–2096[48–50]	9–16[49,50,55]	–
CO linearly adsorbed on Pt{100} terraces	Pt-1	2079	18.3	0.018
	Pt-2	2080	17.3	0.011
	Pt-3	2082	15.6	0.009
	Pt/Al_2O_3	2085[b]	n.d.[c]	n.d.[c]
	lit. values	2075–2084[48–50]	14–20[49,50,55]	–
CO linearly adsorbed on defect sites	Pt-1	2056	44.5	0.012
	Pt-2	2057	45.6	0.009
	Pt-3	2058	44.1	0.008
	Pt/Al_2O_3	2045	n.d.[c]	n.d.[c]
	lit. values	2041–2072[48–50]	25–51[49,64]	–
CO next to metal–support interface	Pt-1	2010	49.7	0.002
	Pt-2	2010	47.9	0.001
	Pt-3	2010	50.2	0.001
	Pt/Al_2O_3	n.d.[c]	n.d.[c]	n.d.[c]
	lit. values	1950–2025[57,65]	"broad" [65]	–
bridged CO on Pt	Pt-1	1868	57.9	0.004
	Pt-2	1865 (1800)[d]	62.4 (50.7)[d]	0.004[d]
	Pt-3	1870	82.2	0.001
	Pt/Al_2O_3	1840	n.d.[c]	n.d.[c]
	lit. values	1780–1882[49,57]	35–50[52,55]	–

[a] fwhm = full width at half-maximum. [b] No deconvolution of terrace sites. [c] n.d. = not determined. [d] Two species.

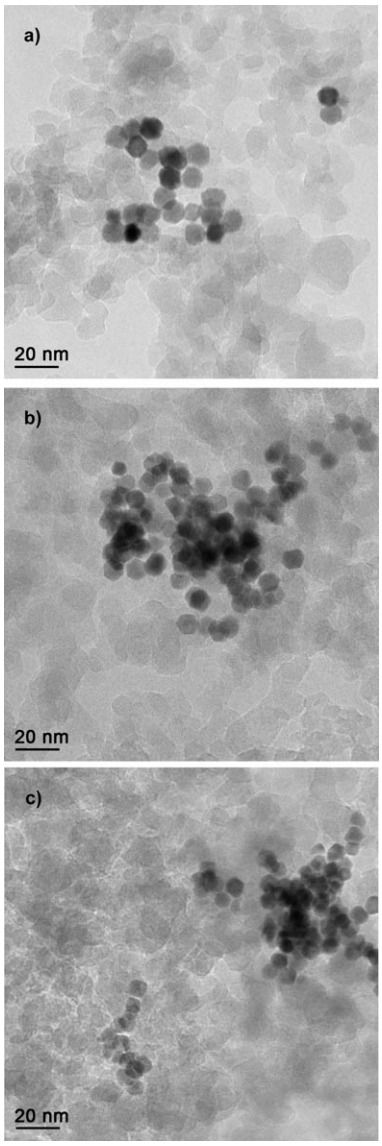

Figure 4. Representative TEM images of the silica-supported nanoparticle Pt-2 after a) hydrogenation of cyclohexene at 1 bar H_2, b) after catalyst pretreatment in O_2 and subsequently in H_2 at 473 K, and c) after cyclohexene hydrogenation at 1 bar H_2 subsequent to the combined oxidative–reductive treatment.

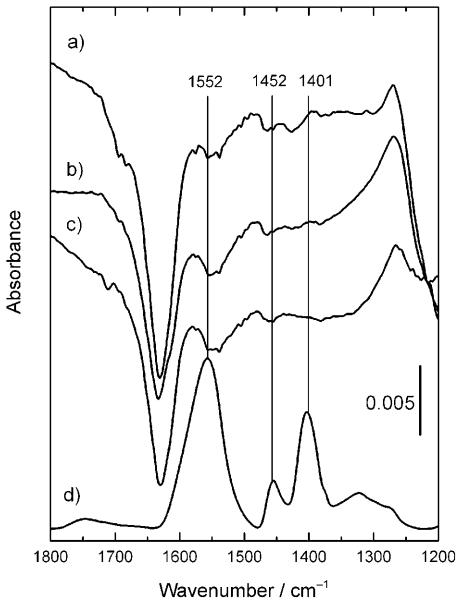

Figure 5. Difference DRIFT spectra derived from the spectra taken after and before the combined oxidative–reductive pretreatment for a) Pt-1, b) Pt-2, and c) Pt-3; d) shows the IR spectrum of the neat stabilizer PAA as sodium salt.

Catalytic behavior of the nanoparticles

Cyclohexene hydrogenation in the liquid phase: The hydrogenation of cyclohexene was used as a test reaction to elucidate the influence of colloid stabilizer on the activity of Pt nanoparticles. The different Pt loadings and metal dispersions of the supported Pt nanoparticles and the reference catalyst Pt/Al_2O_3 were compensated during hydrogenation by applying adjusted amounts of catalysts under otherwise identical conditions (see the Experimental Section). In other words, the molar amount of the substrate related to the amount of surface Pt atoms was kept at a similar value.

The experiments were started by investigating the influence of the reaction temperature on the activity of Pt/Al_2O_3 (see Figure S2 in the Supporting Information). The reaction rate was characterized by the turnover frequency (TOF) related to the number of surface Pt sites. The TOFs were calculated from the slope of the linear part of the conversion–time curves that correspond to 20–80% conversion. The TOFs of 2.23 and 7.80 s^{-1} calculated for 275 and 307 K, respectively, agree well with the values reported for various Pt catalysts under these conditions.[67] The good agreement with the literature data confirms the absence of significant interference by mass transfer below 80% conversion.

Next, the influence of the catalyst pretreatment on the hydrogenation of cyclohexene with Pt/Al_2O_3 is shown in Table 4. In the experiments at 10 bar, the TOFs were calculated from the time needed to achieve 40–60% conversion, that is, assuming linearity in this region. The change in the dispersion of the reference Pt/Al_2O_3 due to pretreatment was negligible and there was only a small improvement in the hydrogenation activity. Our interpretation is that the ref-

Table 4. Influence of oxidative–reductive catalyst pretreatment (+) at 473 K on metal dispersion (D) and rate of cyclohexene hydrogenation at different H_2 pressures.

Catalyst	Pretreatment	D	TOF [s^{-1}]	
			1 bar	10 bar
Pt-1	–	0.14	1.36	4.89
	+	0.12	4.58	7.85
Pt-2	–	0.14	1.56	4.65
	+	0.12	4.44	7.63
Pt-3	–	0.14	1.20	4.53
	+	0.12	4.02	7.26
Pt/Al_2O_3	–	0.32	4.02	8.04
	+	0.30	4.72	8.11

erence Pt/Al_2O_3 contains only minor amounts of surface impurities that do not play a significant role in the hydrogenation reaction, which is in agreement with the results of CO adsorption (see above).

The as-synthesized Pt nanoparticles were less active by a factor of about 2.9 and 1.7 at 1 and 10 bar, respectively, relative to the reference catalyst. Clearly, the poisoning effect of the stabilizer decreases with increasing hydrogen pressure. It is also interesting that the activities of as-prepared Pt nanoparticles correspond to about 30–40% of the activity of Pt/Al_2O_3 at as little as 1 bar, although CO adsorption on the same nanoparticles was almost completely blocked (see above). These observations suggest that PAA is partly removed from the Pt surface by the competitive adsorption of hydrogen in the presence of solvent, whereas this process is not possible at the solid/gas interface during CO chemisorption. Dendrimer-encapsulated nanoparticles showed a similar behavior of reasonable activity in the presence of a solvent,[68,69] although they were inactive for gas-phase reactions.[70]

Boudart and co-workers[67] demonstrated that cyclohexene hydrogenation on Pt is structure-insensitive, independent of the catalyst support, metal loading, and particle size. These and other studies on the structure sensitivity of cyclohexene hydrogenation support our interpretation that the lower activity of the supported nanoparticles compared to that of Pt/Al_2O_3 should be attributed to partial site blocking by the residual stabilizer molecules.[71]

The influence of the pretreatment procedure on the activity of the Pt nanoparticles is highlighted by the calculated TOFs in Table 4 (for conversion versus time plots, see Figure S3 in the Supporting Information). The remarkable rate enhancement is attributed to the efficient cleaning of the metal surface by decarboxylation of the residual PAA, a process that is catalyzed by the Pt surface sites.[63] After the pretreatment, the activity of the nanoparticles approached that of Pt/Al_2O_3 within 5–15% (Table 4). Oxidative removal of the major part of the stabilizer is underlined by the observation of some agglomeration of Pt nanoparticles by electron microscopy (see Figure 4b and c) and the resulting decrease in the dispersion from 0.14 to 0.12 (Table 4). Agglomeration or additional restructuring was not observed by TEM after the hydrogenation of cyclohexene when no catalyst pretreatment was applied (Figure 4a). The good stability of the nanoparticles during liquid-phase hydrogenation at room temperature is probably connected to the effect of strongly adsorbed hydrogen and the negligible change of the catalyst potential during hydrogenation of the olefin. Application under oxidizing conditions or in the presence of a good chelating agent may lead to rapid restructuring of the nanoparticles, as observed by El-Sayed and co-workers.[72]

Hydrogenation of cinchonidine: Cinchonidine, the most commonly used chiral modifier of Pt in the enantioselective hydrogenation of ketones, is not stable on the Pt surface under the usual reaction conditions, in the presence of H_2. The first, facile step of its degradation is the hydrogenation of the vinyl group to afford 10,11-dihydrocinchonidine (CDH_2; Scheme 1). The efficiency of CDH_2 as chiral modifier is about the same as that of CD, but the slow hydrogenation of the quinoline unit weakens its adsorption on Pt and leads to a considerable loss in enantiomeric excess (*ee*).[38,39]

Saturation of the heteroaromatic (pyridine) ring affords two diastereomers ((*R*)- and (*S*)-CDH_6-A) with the opposite absolute configuration at C(4′). The other intermediate CDH_6-B is formed by hydrogenation of the homoaromatic ring. The latter reaction has recently been described as structure sensitive: Pt{100} surfaces on nanoparticles are remarkably more active than Pt{111} faces.[43] Further hydrogenation of the hexahydro derivatives results in up to eight diastereomers of dodecahydrocinchonidine (CDH_{12}). It has also been shown with UV spectroscopy that the rate of hydrogenation of the homo- or heteroaromatic ring strongly depends on the reaction conditions, for example, on the solvent.[40] In nonpolar solvents such as toluene, the hydrogenation of the pyridine ring was observed almost exclusively. In acetic acid, the hydrogenation of the pyridine ring was less dominant.

A typical example of the kinetics of CD hydrogenation is shown in Figure 6. On Pt/Al_2O_3 in acetic acid, the main hexahydro isomer is (*R*)-CDH_6-A (Figure 6B, curve a). Interest-

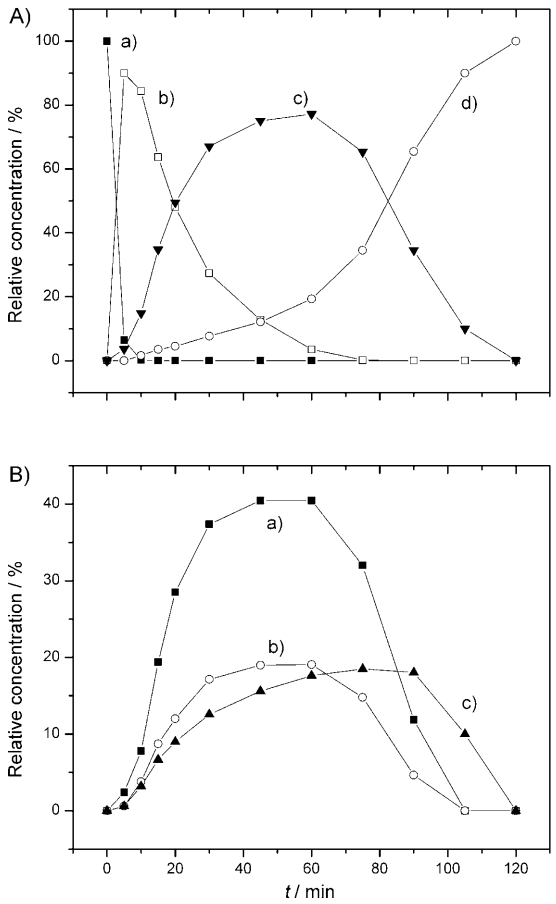

Figure 6. Hydrogenation of CD in acetic acid using the as-received Pt/Al_2O_3 reference catalyst (see also Scheme 1). Part A: a) CD; b) CDH_2; c) CDH_6 (A+B); d) CDH_{12} (8 isomers). Part B: a) (*R*)-CDH_6-A; b) (*S*)-CDH_6-A; c) CDH_6-B.

ingly, further hydrogenation of the two CDH_6-A diastereomers to CDH_{12} is preferred over hydrogenation of CDH_6-B, and thus CDH_6-B accumulates with increasing conversion (Figure 6B). For comparison, UV spectroscopic investigations[40,43] indicated a high selectivity to CDH_6-B (at high conversion of CDH_2), whereas the formation of CDH_6-A was underestimated due to the poor sensitivity of UV spectroscopy for the detection of these isomers in the presence of significant amounts of alkaloid with intact quinoline rings, that is, at low conversion.[40]

The reaction rates (TOFs) and the product distributions are presented in Tables 5 and 6. The selectivities are compared at (40 ± 5)% conversion of CDH_2; at this conversion,

Table 5. Shape selectivity in the hydrogenation of cinchonidine in toluene and the effect of oxidative–reductive catalyst pretreatment (+) at 473 K.

Catalyst	Pretreatment	TOF [h^{-1}]	Selectivity[a] [%]		
			CDH_6-A	CDH_6-B	CDH_{12}
Pt-1	–	7.3	75	14	11
	+	11.6	89	2	9
Pt-2	–	3.7	72	19	9
	+	5.7	91	2	7
Pt-3	–	1.3	80	10	10
	+	2.0	91	1	8
Pt/Al_2O_3	–	6.4	87	3	10
	+	6.7	84	4	12

[a] Determined at (40 ± 5)% conversion of CDH_2.

Table 6. Cinchonidine hydrogenation in acetic acid: Shape selectivity and the effect of oxidative–reductive catalyst pretreatment (+) at 473 K.

Catalyst	Pretreatment	TOF [h^{-1}]	Selectivity[a] [%]		
			CDH_6-A	CDH_6-B	CDH_{12}
Pt-1	–	14.6	74	17	9
	+	15.7	75	16	9
Pt-2	–	7.9	78	15	7
	+	8.8	76	15	9
Pt-3	–	2.1	78	14	8
	+	2.3	79	12	9
Pt/Al_2O_3	–	8.1	68	22	10
	+	8.0	73	17	12

[a] Determined at (40 ± 5)% conversion of CDH_2.

no CD is left in the reaction mixture and the amount of the fully hydrogenated product CDH_{12} is still low. The TOFs are based on the number of Pt surface atoms (see Table 4) and were calculated from the almost linear decrease in the concentration of CDH_2 at low conversion but in the absence of CD (see Figure 6A). Note that all experiments shown in Tables 5 and 6 were repeated with Pt-1 deposited onto Al_2O_3, and the TOFs were on average 10% lower and the selectivities deviated by 0–3% relative to the standard Pt-1 deposited onto silica. Clearly, the support effect is minor and does not affect the comparison of the silica-supported nanoparticles to the reference Pt/Al_2O_3.[43]

Variation of the dominant crystallographic face of the Pt nanoparticles influenced mainly the rate of the reaction (Tables 5 and 6). The TOFs increased in the order Pt-3 < Pt-2 < Pt-1, independent of the solvent and the catalyst pretreatment in oxygen and hydrogen (Tables 5 and 6). This sequence is the same as that obtained with a former qualitative UV spectroscopic analysis, and the probable origin of the change in reactivity is the higher adsorption strength of CD on Pt{100} faces relative to Pt{111} faces, as indicated by DFT calculations.[40,43] The removal of the residual stabilizer increased the rate in toluene by at least 50% (Table 5), which is in good agreement with the results of cyclohexene hydrogenation (Table 4). In contrast, in acetic acid the effect was minor, not exceeding 10% (Table 6). In the case of the relatively clean reference Pt/Al_2O_3, the effect of pretreatment was almost negligible, independent of the solvent. We attribute these differences to the solubility of the residual stabilizer on the nanoparticles: PAA dissolves much better in acetic acid, it is partially removed from the Pt surface during reaction, and thus the site-blocking effect is smaller in that solvent.

A comparison of the performance of Pt/Al_2O_3 in the two solvents shows that the presence of acetic acid increased the chemoselectivity to CDH_6-B by a factor of 4–7 (Tables 5 and 6), which is in agreement with a former UV and NMR spectroscopic study.[40] The shift in the chemoselectivity is due to interaction of the solvent acid with the adsorbed alkaloid, as will be discussed later.

Using the as-prepared Pt nanoparticles the chemoselectivity did not vary significantly when changing the solvent from toluene to acetic acid, in clear contrast to the behavior of Pt/Al_2O_3. Heat treatment of the nanoparticles reduced the chemoselectivity to CDH_6-B in toluene (Table 5) but barely affected it in acetic acid. These changes in the chemoselectivities indicate that PAA, which remains on the Pt surface after preparation, interacts with CD during hydrogenation about as strongly as the solvent acetic acid. Oxidative removal of carboxylic-acid-type surface species eliminates the PAA–CD interaction and the chemoselectivities to CDH_6-A increase to about 90% on all nanoparticles.

Analysis of the diastereoselectivity in CDH_6-A uncovered an even more striking effect of PAA (Figure 7). In toluene,

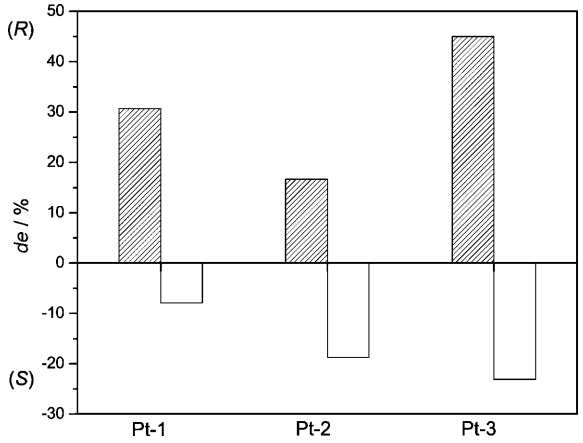

Figure 7. Diastereoselectivity in the hydrogenation of CD to CDH_6-A in toluene with as-prepared nanoparticles (filled columns) and after the combined oxidative–reductive catalyst pretreatment (empty columns).

there is no clear correlation between the crystallographic face of Pt and the diastereomeric excess (*de*) on the as-prepared nanoparticles, but after catalyst pretreatment the *de* inverted from *R* to *S*. In the case of Pt-3, the nanoparticles, which contain predominantly Pt{111} faces, the *de* switched from 45% *R* to 23% *S*. We can conclude that in the absence of an acid—either as a solvent or the colloid stabilizer—the Pt nanoparticles provide (*S*)-CDH_6-A as the major product and the *de* increases with increasing Pt{111}/Pt{100} ratio. In acetic acid, all catalysts gave the (*R*)-diastereomer in excess independent of the catalyst pretreatment, but after pretreatment the *de* increased by about 6–12% (Figure 8). In addition, the *de* increased in the order Pt-1 < Pt-2 < Pt-3, that is,

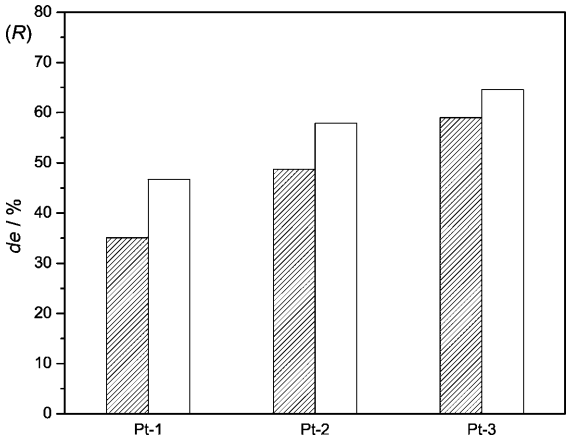

Figure 8. Diastereoselectivity in the hydrogenation of CD to CDH_6-A in acetic acid. Filled columns: as-prepared nanoparticles; empty columns: after oxidative–reductive catalyst pretreatment.

the Pt{111} face is more selective than the Pt{100} in both solvents.

Scheme 2 illustrates two dominant adsorption modes of the alkaloid on the Pt surface, based on former DFT calculations.[34] The so-called surface-open(4) (SO(4)) conformation leads to the formation of (*S*)-CDH_6-A upon hydrogenation of the pyridine moiety, assuming the hydrogen uptake from the Pt surface. Formation of the *R* diastereomer is expected upon hydrogenation of CDH_2 adsorbed on Pt in a so-called surface-open(3) (SO(3)) geometry. A key point here is that the two conformers are not interconvertable without desorption and readsorption of the quinoline ring. Our results demonstrate that the carboxylic acid functional groups of PAA, adsorbed irreversibly on the Pt surface, can invert the dominant adsorption mode of the alkaloid, thereby resulting in the formation of the opposite diastereomer in excess (Figure 7). A probable interaction would involve the strongly basic quinuclidine N atom of the alkaloid, although a weak hydrogen-bonding interaction with the quinoline N atom cannot be excluded. The acidity of PAA is expected to be similar to that of acetic acid ($pK_a = 4.7$), and a considerable excess of acetic acid could protonate the quinuclidine nitrogen ($pK_a = 10.0$), but its interaction with the

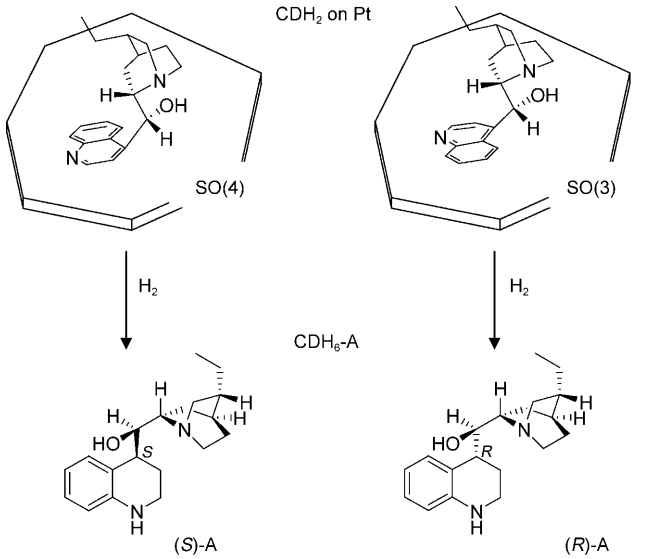

Scheme 2. Schematic illustration of adsorption modes of dihydrocinchonidine (CDH_2) on Pt, thus leading to formation of *S* and *R* isomers of CDH_6-A upon hydrogenation.

quinoline N atom ($pK_a = 5.8$) was barely detectable with NMR spectroscopy.[73]

To our knowledge, this is the first evidence for the control of the diastereoselectivity of a metal nanoparticle through the colloid stabilizer. Recently, Ooe et al. used dendrimer-encapsulated Pd nanoparticles for competitive hydrogenations.[74] The presence of the polar dendrimer on the Pd surface increased the relative reactivity of polar substrates compared to a Pd/C reference catalyst. Clearly, such an effect can be explained by the different solubilities of the substrates,[75] and the phenomenon is different from the direct interaction of the colloid stabilizer and the reactant at the metal surface.

Conclusion

Intrigued by the importance in catalysis of metal nanoparticles that possess special size and shape distributions, we have studied the influence of the crystallographic faces of Pt on the diastereoselective hydrogenation of cinchonidine (CD). Three different Pt nanoparticles with controlled size and shape distributions have been prepared by varying the concentration of PAA, a widely used colloid stabilizer,[21,76] and then the particles were deposited onto silica. All three samples possessed very similar Pt particle size distributions, whereas the particle shapes varied from preferentially cubic (Pt-1) to cubooctahedral (Pt-2) and octahedral (Pt-3), thus corresponding to an increasing {111}/{100} ratio.

DRIFT spectroscopy showed that the majority of the Pt surface sites were blocked by the stabilizer and were not accessible to CO chemisorption at the gas/solid interface. The extended {100} and {111} faces could be freed from PAA by a pretreatment in oxygen and then in hydrogen at 473 K.

The efficient regeneration of the surface sites is attributed to the Pt-catalyzed oxidative decarboxylation of PAA.

In the hydrogenation of cyclohexene in toluene, all as-prepared nanoparticles showed reasonable activity due to the mobility of the stabilizer at the solid/liquid interface. Only a partial poisoning effect was observed compared with the performance of a reference Pt/Al_2O_3 catalyst, and the combined catalyst pretreatment eliminated most of the site-blocking effect of the stabilizer. Note that CD adsorbs even more strongly than cyclohexene on Pt and can efficiently compete with PAA for the surface Pt sites in the presence of a solvent.

Hydrogenation of the aromatic moiety of CD is an important side reaction during the enantioselective hydrogenation of ketones on Pt and an ideal test reaction due to the complex interaction (adsorption) of the alkaloid with the Pt surface. A striking observation is that the diastereoselectivity in the hydrogenation of the pyridine ring of CD is controlled by the crystallographic face of Pt and the strongly adsorbed colloid stabilizer. After removal of the stabilizer, the (*S*)-CDH_6-A diastereomer formed in excess in the weakly interacting solvent toluene and the *de* increased on the Pt{111}-rich samples (Pt-3 > Pt-2 > Pt-1). In the presence of the residual stabilizer at the Pt surface, however, the major diastereomer inverted to (*R*)-CDH_6-A and the unambiguous correlation between the crystallographic face and the diastereoselectivity became indistinct. In acetic acid, both the as-prepared and the pretreated nanoparticles gave the *R* diastereomer in excess and the diastereoselectivity increased again with the increasing Pt{111}/Pt{100} ratio. Variation of the diastereoselectivity indicates that the presence of an acid on the Pt surface inverts the dominant adsorption mode of CD. Clearly, the presence of the stabilizer at the Pt surface induces a "surface-localized acidification", as its influence on the diastereoselectivity is comparable to that of the solvent acetic acid.

A general conclusion emerging from this study is that not only the activity but also the selectivity of colloid-derived nanoparticles may be significantly affected by the residual stabilizer. Possible interactions with the substrate as shown here may have a more complex impact on the catalytic performance than a simple site-blocking effect as previously proposed. Understanding the catalytic behavior of as-prepared nanoparticles requires a consideration of the interactions among all three components: the metal, the stabilizer, and the substrate.

Experimental Section

Materials: In general, analytical grade reagents and solvents were used. Toluene (Fluka, >99.7%) was dried over an activated molecular sieve 4 Å; acetic acid (Acros Organics, 99.8%), cyclohexene (Fluka, >99.5%), and cinchonidine (CD; Fluka, >98% alkaloid) were used as received. The reference catalyst 5 wt% Pt/Al_2O_3 (Engelhard 4759) has been widely used in enantioselective hydrogenation of ketones in the presence of cinchonidine and its behavior after various pretreatments is well known.[77,78]

The synthesis of Pt nanoparticles with controlled size and shape distribution followed a known procedure.[14,43] The starting solution of 0.1 mmol L^{-1} K_2PtCl_4 (Aldrich, >99.9%) and the PAA stabilizer (poly(acrylic acid) sodium salt, Aldrich, average $M_r \approx 2100$) in water (250 mL) was degassed by bubbling Ar (6.0, Pangas) for 1 h and then stirred for 24 h. A high fraction of cubic Pt nanoparticles (Pt-1) with preferentially exposed {100} phases was obtained at a Pt to PAA molar ratio of 1:1. Increasing the concentration of PAA by a factor of 3 (Pt-2) or 5 (Pt-3) at a constant pH of 7 results in a higher fraction of cubooctahedral and octahedral particles, respectively, that feature higher amounts of {111} phases. Precipitation of the colloids onto the nonporous, flame-made support in a nominal loading of 1 wt% Pt was reached by stirring the degassed colloidal solution with a suspension of support material (500 mg) in water (150 mL), followed by the addition of HCl (0.1 M) until a pH of 2 was reached. Generally, silica (Aerosil 200, Degussa, BET surface area: 200 $m^2 g^{-1}$) was used as support, but for Pt-1 the colloidal solution was divided into two fractions that have been deposited onto either silica or Al_2O_3 (aluminum oxide C, Degussa, BET surface area: 100 $m^2 g^{-1}$). After filtration and careful washing with water ten times, the supported Pt nanoparticles were dried at 333 K in vacuum (10 mbar) overnight.

Details on the synthesis and purification of the hydrogenation products of CD and their characterization by ^1H NMR spectroscopy (Bruker 200 MHz) are given in the Supporting Information. The characterization data agreed well with the values given in the literature.[38,39]

Electron microscopy: For TEM investigations, the material was deposited onto a holey carbon foil supported on a copper grid. TEM investigations were performed using a CM30ST microscope (FEI; LaB_6 cathode, operated at 300 kV, point resolution ≈2 Å). Scanning transmission electron microscopy (STEM) images were recorded using a high-angle annular dark field (HAADF) detector at a Tecnai F30 microscope (FEI; field emission gun, operated at 300 kV, point resolution ≈2 Å). HAADF-STEM images reveal the metal particles with bright contrast (*Z* contrast). The particle size and shape distribution as well as the metal dispersion were determined for the three different colloids in aqueous solution and after deposition onto silica, and also for the reference catalyst Pt/Al_2O_3. The measurements were repeated after the catalyst pretreatment and after the catalytic reaction.

Atomic absorption spectroscopy (AAS): AAS was used for the determination of the Pt content of the catalysts. All measurements were performed using a Varian SpectrAA 220 FS spectrometer equipped with an air/C_2H_2 burner and a D_2 lamp for background correction. The samples were dissolved in a HF/aqua regia mixture overnight.

X-ray photoelectron spectroscopy (XPS): XPS analysis of the Pt nanoparticles deposited onto silica was performed using a Leybold Heraeus LHS11 MCD instrument with $Mg_{K\alpha}$ (1253.6 eV) radiation. The sample was pressed into a sample holder, evacuated in a load lock to 10^{-6} mbar, and transferred to the analysis chamber (typical pressure $<10^{-9}$ mbar). The peaks were energy-shifted to the binding energy of Si 2p for silica (103.4 eV) to correct for the charging of the material. The surface composition of the catalysts was determined from the peak areas of Pt 4f, Si 2p, O 1s, Cl 2s, and C 1s, which were computed after subtraction of the Shirley-type background by empirically derived cross-section factors.

DRIFTS study of CO adsorption: Adsorption of CO from the gas phase was used as a standard method to characterize the catalytic materials. A varying dilution of the samples in KBr (1:20–1:2) was used to account for the different Pt loadings. Prior to adsorption, the samples were placed into the reaction chamber (HVC-DRPZ, Harrick) and dried in flowing Ar (20 mL min^{-1}) at 298 K for 60 min. The following pretreatment procedure was applied: oxidation in flowing O_2 at 473 K for 1 h, purging with Ar for 5 min followed by reduction in H_2 at a constant temperature for an additional 1 h. After cooling to 298 K the samples were purged in flowing Ar for 30 min followed by adsorption of CO (10% in He) at a flow rate of 20 mL min^{-1}. An adsorption time of 90 min was found to be sufficient to observe saturation coverage. After removal of the gas phase CO from the cell by purging with Ar, DRIFT spectra were recorded using a Bruker Equinox 55 spectrometer equipped with a liquid-nitrogen-cooled MCT detector. Spectra were collected by coaddition of 500 scans at a scanner velocity of 10 kHz and a resolution of 4 cm^{-1}.

Liquid-phase hydrogenation of cyclohexene: Hydrogenation of cyclohexene (160 mg, 1.95 mmol) in toluene (5 mL) at 298 K and 10 bar hydrogen was performed in a stainless steel reactor equipped with a glass liner, polytetrafluoroethylene (PTFE) cover, and magnetic stirrer (750 rpm). Pressure was controlled using a constant-volume constant-pressure system (Büchi BPC 9901). The amount of catalyst was either 10 mg of Pt-1, Pt-2 or Pt-3 (1 wt% Pt) or 2 mg of Pt/Al_2O_3 (5 wt% Pt) to account for the different Pt loadings. Reactions at ambient pressure were carried out in a magnetically stirred glass reactor and scaled up by a factor of four (640 mg cyclohexene and 40 or 8 mg catalyst). Prior to use, the catalysts were dried overnight at 333 K (10 mbar) or pretreated by oxidation in flowing O_2 at 473 K for 1 h, then purged with Ar for 5 min, followed by reduction in H_2 at constant temperature for 1 h. The products were analyzed by gas chromatography (Thermo Quest Trace 2000, HP-FFAP capillary column, FID detector).

Liquid-phase hydrogenation of cinchonidine: Hydrogenation of CD (5 mg, 17 μmol) in solvent (10 mL toluene or acetic acid) at 298 K and 2 bar hydrogen was performed in the stainless steel reactor described above. The amount of catalyst was either 50 mg of Pt-1, Pt-2, or Pt-3 (1 wt% Pt) or 10 mg of Pt/Al_2O_3 (5 wt% Pt) to keep the molar ratio of substrate to surface Pt atoms at around 20. Prior to use, the catalysts were dried overnight at 333 K (10 mbar) or pretreated by oxidation in flowing O_2 at 473 K for 1 h, then purged with Ar for 5 min, followed by reduction in H_2 at constant temperature for an additional 1 h. The samples taken from the reaction mixture were either washed with aqueous 0.1 M NaOH (solvent: toluene) or carefully neutralized by an excess of aqueous 1 M NaOH (solvent: acetic acid) and extracted with toluene three times before being filtered and analyzed by gas chromatography (Thermo Quest Trace 2000, HP-5 capillary column, FID detector). Details on the preparation and characterization of hydrogenated CD derivatives are given in the Supporting Information.

Acknowledgements

Financial support by the Swiss National Science Foundation is kindly acknowledged. The authors like to thank the electron microscopy center of ETH Zürich (EMEZ).

[1] C. Burda, X. B. Chen, R. Narayanan, M. A. El-Sayed, *Chem. Rev.* **2005**, *105*, 1025–1102.
[2] M. J. Yacamàn, J. A. Ascencio, H. B. Liu, J. Gardea-Torresdey, *J. Vac. Sci. Technol. B* **2001**, *19*, 1091–1103.
[3] L. Guczi, G. Peto, A. Beck, Z. Paszti, *Top. Catal.* **2004**, *29*, 129–138.
[4] G. Schmid, *Chem. Rev.* **1992**, *92*, 1709–1727.
[5] D. Astruc, F. Lu, J. R. Aranzaes, *Angew. Chem.* **2005**, *117*, 8062–8083; *Angew. Chem. Int. Ed.* **2005**, *44*, 7852–7872.
[6] Y. S. Shon, H. Choo, *C. R. Chim.* **2003**, *6*, 1009–1018.
[7] A. Roucoux, J. Schulz, H. Patin, *Chem. Rev.* **2002**, *102*, 3757–3778.
[8] J. D. Aiken, R. G. Finke, *J. Mol. Catal. A* **1999**, *145*, 1–44.
[9] Y. Li, M. A. El-Sayed, *J. Phys. Chem. B* **2001**, *105*, 8938–8943.
[10] A. Henglein, B. G. Ershov, M. Malow, *J. Phys. Chem.* **1995**, *99*, 14129–14136.
[11] D. G. Duff, P. P. Edwards, B. F. G. Johnson, *J. Phys. Chem.* **1995**, *99*, 15934–15944.
[12] M. Boutonnet, J. Kizling, V. Mintsa-Eya, A. Choplin, R. Touroude, G. Maire, P. Stenius, *J. Catal.* **1987**, *103*, 95–104.
[13] D. N. Furlong, A. Launikonis, W. H. F. Sasse, J. V. Sanders, *J. Chem. Soc. Faraday Trans. 1* **1984**, *80*, 571–588.
[14] T. S. Ahmadi, Z. L. Wang, T. C. Green, A. Henglein, M. A. El-Sayed, *Science* **1996**, *272*, 1924–1926.
[15] H. Lee, S. E. Habas, S. Kweskin, D. Butcher, G. A. Somorjai, P. Yang, *Angew. Chem.* **2006**, *118*, 7988–7992; *Angew. Chem. Int. Ed.* **2006**, *45*, 7824–7828.
[16] Y. Zhang, M. E. Grass, S. E. Habas, F. Tao, T. Zhang, P. Yang, G. A. Somorjai, *J. Phys. Chem. C* **2007**, *111*, 12243–12253.
[17] T. Teranishi, R. Kurita, M. Miyake, *J. Inorg. Organomet. Polym. Mater.* **2000**, *10*, 145–156.
[18] H. Song, F. Kim, S. Connor, G. A. Somorjai, P. Yang, *J. Phys. Chem. B* **2005**, *109*, 188–193.
[19] C. Wang, H. Daimon, T. Onodera, T. Koda, S. Sun, *Angew. Chem.* **2008**, *120*, 3644–3647; *Angew. Chem. Int. Ed.* **2008**, *47*, 3588–3591.
[20] Y. Zhang, M. E. Grass, J. N. Kuhn, F. Tao, S. E. Habas, W. Huang, P. Yang, G. A. Somorjai, *J. Am. Chem. Soc.* **2008**, *130*, 5868–5869.
[21] M. Inaba, M. Ando, A. Hatanaka, A. Nomoto, K. Matsuzawa, A. Tasaka, T. Kinumoto, Y. Iriyama, Z. Ogumi, *Electrochim. Acta* **2006**, *52*, 1632–1638.
[22] I. Lee, F. Delbecq, R. Morales, M. A. Albiter, F. Zaera, *Nat. Mater.* **2009**, *8*, 132–138.
[23] G. L. Haller, D. E. Resasco, *Adv. Catal.* **1989**, *36*, 173–235.
[24] K. Hayek, R. Kramer, Z. Paal, *Appl. Catal. A* **1997**, *162*, 1–15.
[25] B. L. Mojet, J. T. Miller, D. E. Ramaker, D. C. Koningsberger, *J. Catal.* **1999**, *186*, 373–386.
[26] G. L. Haller, *J. Catal.* **2003**, *216*, 12–22.
[27] M. K. Oudenhuijzen, J. A. von Bokhoven, J. T. Miller, D. E. Ramaker, D. C. Koningsberger, *J. Am. Chem. Soc.* **2005**, *127*, 1530–1540.
[28] A. Y. Stakheev, L. M. Kustov, *Appl. Catal. A* **1999**, *188*, 3–35.
[29] C. H. Bartholomew, *Appl. Catal. A* **2001**, *212*, 17–60.
[30] T. Mallat, E. Orglmeister, A. Baiker, *Chem. Rev.* **2007**, *107*, 4863–4890.
[31] M. Bartók, *Curr. Org. Chem.* **2006**, *10*, 1533–1567.
[32] H.-U. Blaser, M. Studer, *Acc. Chem. Res.* **2007**, *40*, 1348–1356.
[33] D. Y. Murzin, P. Mäki-Arvela, E. Toukoniitty, T. Salmi, *Catal. Rev. Sci. Eng.* **2005**, *47*, 175–256.
[34] A. Vargas, G. Santarossa, M. Iannuzzi, A. Baiker, *J. Phys. Chem. C* **2008**, *112*, 10200–10208.
[35] J. Kubota, F. Zaera, *J. Am. Chem. Soc.* **2001**, *123*, 11115–11116.
[36] A. Kraynov, A. Suchopar, L. D'Souza, R. Richards, *Phys. Chem. Chem. Phys.* **2006**, *8*, 1321–1328.
[37] D. Ferri, T. Bürgi, *J. Am. Chem. Soc.* **2001**, *123*, 12074–12084.
[38] G. Szöllösi, P. Forgó, M. Bartók, *Chirality* **2003**, *15*, S82–S89.
[39] H. U. Blaser, H. P. Jalett, W. Lottenbach, M. Studer, *J. Am. Chem. Soc.* **2000**, *122*, 12675–12682.
[40] W.-R. Huck, T. Bürgi, T. Mallat, A. Baiker, *J. Catal.* **2003**, *216*, 276–287.
[41] R. van Hardeveld, F. Hartog, *Surf. Sci.* **1969**, *15*, 189–230.
[42] R. van Hardeveld, A. van Montfoort, *Surf. Sci.* **1966**, *4*, 396–430.
[43] E. Schmidt, A. Vargas, T. Mallat, A. Baiker, *J. Am. Chem. Soc.* **2009**, *131*, 12358–12367.
[44] J. C. Serrano-Ruiz, A. López-Cudero, J. Solla-Gullón, A. Sepúlveda-Escribano, A. Aldaz, F. Rodríguez-Reinoso, *J. Catal.* **2008**, *253*, 159–166.
[45] C. D. Wagner, A. V. Naumkin, A. Kraut-Vass, J. W. Allison, C. J. Powell, J. J. R. Rumble in *NIST X-ray Photoelectron Spectroscopy Database*, U.S. Dept. of Commerce, National Institute of Standards and Technology, Gaithersburg, **2000**.
[46] A. C. Yang, C. W. Garland, *J. Phys. Chem.* **1957**, *61*, 1504–1512.
[47] R. P. Eischens, W. A. Pliskin, S. A. Francis, *J. Chem. Phys.* **1954**, *22*, 1786–1787.
[48] R. G. Greenler, K. D. Burch, K. Kretzschmar, R. Klauser, A. M. Bradshaw, B. E. Hayden, *Surf. Sci.* **1985**, *152/153*, 338–345.
[49] M. J. Kappers, J. H. van der Maas, *Catal. Lett.* **1991**, *10*, 365–374.
[50] R. K. Brandt, M. R. Hughes, L. P. Bourget, K. Truszkowska, R. G. Greenler, *Surf. Sci.* **1993**, *286*, 15–25.
[51] H. Härle, W. Metka, H.-R. Volpp, J. Wolfrum, *Phys. Chem. Chem. Phys.* **1999**, *1*, 5059–5064.
[52] P. Gardner, R. Martin, M. Tüshaus, A. M. Bradshaw, *J. Electron Spectrosc. Relat. Phenom.* **1990**, *54/55*, 619–628.
[53] M. Tüshaus, E. Schweizer, P. Hollins, A. M. Bradshaw, *J. Electron Spectrosc. Relat. Phenom.* **1987**, *44*, 305–316.
[54] H. Hopster, H. Ibach, *Surf. Sci.* **1978**, *77*, 109–117.
[55] H.-J. Krebs, H. Lüth, *Appl. Phys.* **1977**, *14*, 337–342.
[56] H. Borchert, D. Fenske, J. Kolny-Olesiak, J. Parisi, K. Al-Shamery, M. Bäumer, *Angew. Chem.* **2007**, *119*, 2981–2984; *Angew. Chem. Int. Ed.* **2007**, *46*, 2923–2926.

[57] P. Hollins, *Surf. Sci. Rep.* **1992**, *16*, 51–94.
[58] T. Wang, C. Lee, L. D. Schmidt, *Surf. Sci.* **1985**, *163*, 181–197.
[59] A.-C. Shi, R. I. Masel, *J. Catal.* **1989**, *120*, 421–431.
[60] A. S. Ramachandran, S. L. Anderson, A. K. Datye, *Ultramicroscopy* **1993**, *51*, 282–297.
[61] R. G. Greenler, J. A. Dudek, D. E. Beck, *Surf. Sci.* **1984**, *145*, L453L458.
[62] M. Bartók, J. Sárkány, A. Sitkei, *J. Catal.* **1981**, *72*, 236–245.
[63] H. T. Gomes, P. Serp, P. Kalck, J. L. Figueiredo, J. L. Faria, *Top. Catal.* **2005**, *33*, 59–68.
[64] S. Park, S. A. Wasileski, M. J. Weaver, *J. Phys. Chem. B* **2001**, *105*, 9719–9725.
[65] R. Barth, R. Pitchai, R. L. Anderson, X. E. Verykios, *J. Catal.* **1989**, *116*, 61–70.
[66] W. L. Manner, A. R. Bishop, G. S. Girolami, R. G. Nuzzo, *J. Phys. Chem. B* **1998**, *102*, 8816–8824.
[67] R. J. Madon, J. P. O'Connell, M. Boudart, *AIChE J.* **1978**, *24*, 904–911.
[68] D. Liu, J. Gao, C. J. Murphy, C. T. Williams, *J. Phys. Chem. B* **2004**, *108*, 12911–12916.
[69] R. W. J. Scott, O. M. Wilson, R. M. Crooks, *J. Phys. Chem. B* **2005**, *109*, 692–704.
[70] H. Lang, R. A. May, B. L. Iversen, B. D. Chandler, *J. Am. Chem. Soc.* **2003**, *125*, 14832–14836.
[71] D. E. Gardin, X. Su, P. S. Cremer, G. A. Somorjai, *J. Catal.* **1996**, *158*, 193–198.
[72] R. Narayanan, C. Tabor, M. A. El-Sayed, *Top. Catal.* **2008**, *48*, 60–74.
[73] W.-R. Huck, T. Bürgi, T. Mallat, A. Baiker, *J. Catal.* **2001**, *200*, 171–180.
[74] M. Ooe, M. Murata, T. Mizugaki, K. Ebitani, K. Kaneda, *Nano Lett.* **2002**, *2*, 999–1002.
[75] P. G. J. Koopman, H. M. A. Buurmans, A. P. G. Kieboom, H. von Bekkum, *Recl.: J. R. Neth. Chem. Soc.* **1981**, *100*, 156–161.
[76] J. M. Petroski, Z. L. Wang, T. C. Green, M. A. El-Sayed, *J. Phys. Chem. B* **1998**, *102*, 3316–3320.
[77] R. Hess, F. Krumeich, T. Mallat, A. Baiker, *Catal. Lett.* **2004**, *92*, 141–148.
[78] T. Mallat, S. Frauchiger, P. J. Kooyman, M. Schürch, A. Baiker, *Catal. Lett.* **1999**, *63*, 121–126.

Received: September 11, 2009
Published online: December 28, 2009

